Utility of 7 Tesla MRI for Preoperative Planning of Endoscopic Endonasal Surgery for Pituitary Adenomas

John W. Rutland[1,2] Bradley N. Delman[1,3] Rebecca E. Feldman[1] Nadejda Tsankova[4] Hung-Mo Lin[5] Francesco Padormo[1,6] Raj K. Shrivastava[2,*] Priti Balchandani[1,*]

[1] Translational and Molecular Imaging Institute, Icahn School of Medicine at Mount Sinai, New York, New York, United States
[2] Department of Neurosurgery, Icahn School of Medicine at Mount Sinai, New York, New York, United States
[3] Department of Radiology, Icahn School of Medicine at Mount Sinai, New York, New York, United States
[4] Department of Pathology, Icahn School of Medicine at Mount Sinai, New York, New York, United States
[5] Department of Population Health Science and Policy, Mount Sinai Hospital, New York, New York, United States
[6] Department of Medical Physics, Guy's and St Thomas' NHS Foundation Trust, London, United Kingdom

Address for correspondence John W. Rutland, BA, Department of Neurosurgery, Icahn School of Medicine at Mount Sinai, 1468 Madison Avenue; Floor 8, New York, NY 10129, United States (e-mail: jack.rutland@icahn.mssm.edu).

J Neurol Surg B 2021;82:303–312.

Abstract

Objective There is increasing interest in investigating the utility of 7 Tesla (7 T) magnetic resonance imaging (MRI) for imaging of skull base tumors. The present study quantifies visualization of tumor features and adjacent skull base anatomy in a homogenous cohort of pituitary adenoma patients.

Methods Eighteen pituitary adenoma patients were scanned at 7 T in this prospective study. All patients had reference standard-of-care clinical imaging at either 3 T (7/18, 39%) or 1.5 T (11/18, 61%). Visualization of tumor features and conspicuity of arteries and cranial nerves (CNs) was rated by an expert neuroradiologist on 7 T and clinical field strength MRI. Overall image quality and severity of image artifacts were also characterized and compared.

Results Ability to visualize tumor features did not differ between 7 T and lower field MRI. Cranial nerves III, IV, and VI were better detected at 7 T compared with clinical field strength scans. Cranial nerves III, IV, and VI were also better detected at 7 T compared with only 1.5 T, and CN III was better visualized at 7 T compared with 3 T MRI. The ophthalmic arteries and posterior communicating arteries (PCOM) were better detected at 7 T compared with clinical field strength imaging. The 7 T also provided better visualization of the ophthalmic arteries compared with 1.5 T scans.

Conclusion This study demonstrates that 7 T MRI is feasible at the skull base and identifies various CNs and branches of the internal carotid artery that were better visualized at 7 T. The 7 T MRI may offer important preoperative information that can help to guide resection of pituitary adenoma and reduce operative morbidity.

Keywords
- 7 Telsa MRI
- pituitary adenoma
- endoscopic endonasal surgery
- skull base anatomy
- neurosurgery

* *Co-last authors*

received
June 22, 2019
accepted after revision
September 28, 2019
published online
November 21, 2019

Georg Thieme Verlag KG,
Rüdigerstraße 14,
70469 Stuttgart, Germany

DOI https://doi.org/10.1055/s-0039-3400222.
ISSN 2193-6331.

Introduction

Pituitary adenomas are benign skull base tumors that account for 10 to 15% of all intracranial neoplasms.[1] Endoscopic endonasal surgery (EES) is the initial treatment strategy for most adenomas, although prolactinomas are typically first treated with medical therapy. Advantages of EES over traditional approaches include panoramic visualization of the anterior skull base, diminished brain retraction, and reduced need for cranial disassembly. Advanced neuronavigation platforms and high-resolution preoperative imaging are critical in intraoperative decision making and endoscopic approach. The anatomical complexity of the anterior skull base and proximity of tumor to vital neurovascular structures can hamper gross-total resection. Furthermore, extensive bony, orbital, dural, and vascular tumor involvement can complicate surgical access to the sella, thereby increasing risk for significant surgery-related morbidity. Surgical complications, which are not uncommon, may include vision loss, endocrine dysfunction, cranial neuropathy, postoperative cerebrospinal fluid (CSF) leak, and infection.[2–6] To optimize surgical planning and navigation, and to facilitate favorable treatment outcomes for patients undergoing EES, high-resolution preoperative magnetic resonance imaging (MRI) has become essential for optimal identification of small skull base structures, as well as differentiation of healthy gland from tumor.[7–9]

Ultra-high-field MRI is increasingly being applied to the study of neurological disease.[10] The 7 Tesla (7 T) MRI has evolved from a research tool to an FDA (Food and Drug Administration)-approved modality with diverse applications. Advantages of 7 T MRI over conventional field strengths (hereafter "conventional-MRI" primarily at 1.5 and 3 T) include increased spatial resolution, signal-to-noise ratio (SNR), and resolution. There is growing interest in exploiting imaging at 7 T to characterize structures and processes for various disease profiles including nonlesional epilepsy,[11] multiple sclerosis,[12] and Alzheimer's disease.[13] However, few studies have employed 7 T MRI to image skull base tumors, in part due to physical complexities of imaging in close proximity to bone and air-filled cavities in the skull base. de Rotte et al first reported the feasibility of pituitary imaging at 7 T MRI.[9] Barrett et al, who qualitatively compared 7 T versus conventional MRI in a preliminary set of skull base patients, confirmed improved detection rates of internal carotid artery (ICA) branches and cranial nerves (CNs) at 7 T.[14] Most recently, Law et al reported results from a microadenoma in one Cushing's patient who was MRI negative at conventional field strength but visible at 7 T in a location that correlated with petrosal sampling and postoperative outcome.[15]

Early reports suggesting feasibility and benefits of ultra-high field MRI over lower field techniques in pituitary pathology have been limited by small sample sizes and inability to statistically compare 7 T to lower field scans.[9,14] Furthermore, the utility of 7 T MRI has not been quantitatively examined in a homogenous cohort of pituitary adenoma patients. The purpose of the present study was to acquire preoperative 7 T MRI and quantitatively compare detailed neuroradiological findings for pituitary adenomas and adjacent skull base neurovascular structures to conventionl MRI. Findings from this study may indicate which structures 7 T scans visualize to greater advantage. In the process, this assessment may help define the role of 7 T in the diagnostic workup of patients with pituitary tumors, and perhaps broader skull base tumors in general.

Methods

Participants

Approval was obtained from the Mount Sinai Medical Center Sinai Institutional Review Board, and all patients provided written informed consent. Eighteen patients with pituitary adenomas were recruited through their neurosurgeon (RKS), and were scanned at 7 T MRI between September 2014 and July 2018 at the Mount Sinai Medical Center. Prior surgical or radiotherapeutic intervention was exclusionary, and ultimate diagnosis was confirmed histologically.

Imaging

Participants were scanned using a 7 T whole-body MRI scanner (Magnetom, Siemens Healthcare, Erlangen, Germany). A SC72CD gradient coil was used ($G_{max} = 70$ mT/m, max slew rate = 200 T/m/s), with a single-channel transmit and 32-channel receive head coil (Nova Medical, Wilmington, Massachusetts, United States). Scanning parameters are presented in ►**Table 1**. All participants also underwent preoperative conventional-MRI at a lower field strength (1.5 T/3 T) obtained per standard of care.

Image Rating

Tumors and surrounding structures were rated by an expert neuroradiologist (BND) with over 20 years in neuroradiology and significant 7 T MRI experience. Tumor features were rated 0 to 4, with 0 indicating nonvisualization, and 1 to 4 indicating poor, fair, good, and excellent visualization, respectively. Internal tumor characteristics, surrounding CNs, and adjacent branches of the internal carotid arteries (ICAs) were ranked on this scale at both 7 T and clinical field strength MRI. Knosp's scores were also determined at 7 T and conventional MRI.

In addition to characterization of tumor features and visibility of image skull base anatomy, 7 T and conventional MRI were also rated for overall diagnostic quality and presence of artifacts. MPRAGE, MP2RAGE, axial T2-TSE, coronal T2-TSE, diffusion, and TOF images were each scored 0 to 2, reflecting nondiagnostic, diagnostic with limitations, and fully diagnostic scans, respectively. Each acquisition sequence was also evaluated for artifact from B1 inhomogeneity, B0 inhomogeneity, motion, and pulsation were rated from 0 to 4, reflecting no, minor, moderate, and severe artifacts, respectively. Tumor measurements in transverse, anterior/posterior, and craniocaudal dimensions were used to calculated volumes using a validated ellipsoid formula[16] ($V = \pi/6 \times [T \times AP \times CC]$).

Statistics

Statistical analyses were calculated using SAS v9.4 (SAS Institute Inc., Cary, North Carolina, United States). Two-tailed signed rank *t*-tests assessed differences between results at 7 T and clinical field strength imaging (1.5 and 3 T combined).

Table 1 7 Tesla imaging protocol

	MPRAGE	MP2RAGE	T2-TSE	DWI	T2-TSE	TOF
Orientation	Coronal oblique	Axial	Coronal oblique	Coronal oblique	Axial	Coronal oblique
Scan time (min:s)	7:40	8:08	6:50	9:19 (18:38[a])	6:50	10:13
Voxel size (mm^3)	$0.7 \times 0.7 \times 0.7$	$0.7 \times 0.7 \times 0.7$	$0.4 \times 0.4 \times 2.0$	$1.05 \times 1.05 \times 1.05$	$0.4 \times 0.4 \times 2.0$	$0.35 \times 0.26 \times 0.4$
Slice number (slabs)	224	240	60	66	55	240(4)
FOV (mm^2)	225×169	224×168	200×168	210×210	200×168	200×170
2D/3D	3D	3D	2D	2D	2D	3D
TR (ms)	3,000	6,000	6,000	7,200	6,000	18.0
TE (ms)	4.1	3.62	59	67.6	59	5.58
TI (TI2; ms)	1,050	1,050 (3,000)	N/A		N/A	
Flip angle (2nd flip angle; degree)	7	5(4)	180	180	180	20
Resolution	320×240	320×240	512×432	200×200	512×432	768×491
Directions	N/A	N/A	N/A	64	N/A	N/A

Abbreviations: 2D, two-dimensional; 3D, three-dimensional; DWI, diffusion-weighted imaging; FOV, field of view; MPRAGE, magnetization prepared rapid acquisition with gradient echo; N/A, not available; T2-TSE, T2-weighted turbo spin echo; TE, echo time; TI, inversion time; TOF, time of flight; TR, repetition time.
[a]Diffusion was acquired with both anterior-posterior and posterior–anterior readout directions.

Identical statistical subanalyses compared 7 T with 3 T ($n = 7$), and 7 T with 1.5 T ($n = 11$). Spearman's correlation coefficient assessed the relationship between overall diagnostic image quality and tumor volume. A false discovery rate (FDR) adjustment was used to account for multiple comparisons within each imaging category. FDR-adjusted p-values of <0.05 were considered significant.

Results

Patients

Eighteen patients (12 females, age mean ± SD = 45.2 ± 14.1 years) underwent 7 T MRI. All patients received conventional MRI as part of their diagnostic workup, with 7/11 (39%) undergoing 3 T and 11/17 (61%) 1.5 T scanning. All participants subsequently underwent EES, with one requiring subsequent craniotomy. Immunohistochemistry of surgical specimens revealed 11 null type, 3 gonadotrophs, 2 prolactinomas, 1 growth hormone-secreting, and 1 adrenocorticotrophic hormone (ACTH)-secreting adenoma. Fifteen tumors were macroadenomas and three were microadenomas. Patient demographics and disease features are shown in ►**Table 2**.

Depiction of Tumor Features

Ability to visualize brain invasion, cavernous sinus wall invasion, orbital involvement, chiasm compression, cystic component, tumor extension through bone, and internal tumor vasculature did not differ when evaluating 7 T versus all conventional MRI, or 3 or 1.5 T separately (►**Table 3**).

Cranial Nerves

Compared with clinical field strength MRI, 7 T better detected CN III (Mean [M] = 3.25 vs. 2.37, $p = 0.002$), CN IV (M = 0.84 vs. 0.09, $p = 0.002$), and CN VI (M = 0.95 vs. 0.52, $p = 0.01$; ►**Fig. 1**). CN III was better visualized at 7 T compared with 3 T (M = 3.08 vs. 2.5, $p = 0.03$). CN III (M = 3.36 vs. 2.28, $p = 0.03$), CN IV (M = 0.78 vs. 0.0, $p = 0.04$), and CN VI (M = 0.96 vs. 0.38, $p = 0.03$) were better detected at 7 T compared with 1.5 T MRI (►**Fig. 2**). Results are summarized in ►**Table 3**.

Internal Carotid Artery Branches

Compared with conventional MRI, 7 T better detected ophthalmic arteries (M = 2.5 vs. 1.48, $p = 0.03$) and posterior communicating arteries (PCOMs; M = 2.72 vs. 2.2, $p = 0.03$). Ophthalmic arteries were also better detected at 7 T than at 1.5 T MRI (M = 2.91 vs. 1.27, $p = 0.01$; ►**Table 3**). Conspicuity of ophthalmic arteries and PCOMs at 7 T compared with 1.5 T is shown in ►**Fig. 3**.

Overall Image Quality and Artifact

7 T B0 artifact was greater than on conventional MRI for axial ($p < 0.01$) and coronal ($p < 0.01$) T2-TSE. These findings persisted when evaluating the 7 T and 1.5 T groups for axial ($p = 0.01$) and coronal ($p = 0.003$) T2-TSE images but not when comparing against 3 T ($p > 0.05$ for both sequences). The 7 T B1 artifact was also greater compared with conventional MRI for axial ($p < 0.001$) and coronal ($p < 0.001$) T2-TSE. These findings persisted when evaluating the 7 and 1.5 T groups for axial ($p = 0.01$) and coronal ($p = 0.003$) T2-TSE images. B1 artifact for axial and coronal T2-TSE sequences was also greater at 7 T compared with 3 T ($p = 0.04$ for both sequences; ►**Fig. 4**). Motion artifact was greater at 7 T compared with conventional MRI on axial ($p = 0.001$) and coronal ($p = 0.001$) T2-TSE. These findings persisted when comparing 7 and 1.5 T groups for axial T2-TSE ($p = 0.02$) but not on coronal T2-TSE ($p > 0.05$). There

Table 2 Demographic and disease features of 18 patients with pituitary adenoma

Patient no.	Sex	Age at scan (y)	Classification	Tumor volume (cm^3)	Histo type
1	M	68	Macroadenoma	4.39	Null cell type
2	F	51	Macroadenoma	1.58	Null cell type
3	M	41	Macroadenoma	7.2	Gonadotroph cell type
4	M	47	Macroadenoma	18.25	Gonadotroph cell type
5	F	56	Macroadenoma	18.35	Gonadotroph cell type
6	F	75	Macroadenoma	168	Null cell type
7	M	54	Macroadenoma	0.85	GH cell type
8	F	29	Microadenoma	0.65	Null cell type
9	F	30	Microadenoma	0.34	Prolactinoma
10	F	50	Microadenoma	0.15	Null cell type
11	F	19	Macroadenoma	4.16	Null cell type
12	F	53	Macroadenoma	6.43	Null cell type
13	F	45	Macroadenoma	0.88	Null cell type
14	F	32	Macroadenoma	78.26	Null cell type
15	F	35	Macroadenoma	3.42	Null cell type
16	M	50	Macroadenoma	27.88	Null cell type
17	M	46	Macroadenoma	19.86	Prolactinoma
18	F	33	Macroadenoma	18.85	ACTH cell type

Abbreviations: ACTH, adrenocorticotrophic hormone; F, female; GH, growth hormone; M, male.

were no significant differences in motion artifact between 7 and 3 T ($p > 0.05$ for all sequences). Lastly, pulsation artifact was greater at 7 T compared with conventional MRI for both axial ($p = 0.001$) and coronal ($p = 0.001$) T2-TSE. These findings persisted when evaluating the 7 and 1.5 T groups for axial T2-TSE ($p = 0.02$), and coronal ($p = 0.02$) T2-TSE but not when comparing 7 T with 3 T ($p > 0.05$ for both sequences).

There were no significant differences in overall diagnostic quality at 7 T compared with conventional MRI ($p > 0.05$ for all sequences), and when comparing 7 to 3 and 1.5 T separately. There was a significant positive correlation between overall image quality and tumor volume for the 7 T images ($r = 0.6$, $p < 0.01$).

Discussion

Proximity of pituitary adenomas to sensitive neurovascular structures confers surgical complexities, especially in EES where maneuverability within narrow surgical corridors can be limited. High-resolution preoperative imaging of CNs and ICA branches is critical in preoperative planning and intraoperative decision making. While many of these structures are well characterized with conventional MRI, visualization of finer anatomy may be challenging. This study confirmed that certain skull base structures are better visualized at 7 T MRI than on conventional MRI, suggesting that ultra-high field imaging could play an increasing role in the treatment algorithm for pituitary adenomas and other skull base lesions.

Imaging the Cranial Nerves

Preoperative identification of delicate CNs is crucial for endoscopic navigation, since disruption can cause significant morbidity. Literature reveals considerable interest in characterization of CNs in assessment of various skull base pathologies, including pituitary adenomas,[7,14] trigeminal neuralgia,[17–19] vestibular schwannomas,[20,21] and among others.[22] Those studies have examined conventional imaging[7,17,18] and advanced sequences, such as diffusion tensor imaging (DTI)[19–22] in CN assessment. This study indicates that several CNs are better imaged at 7 T MRI compared with conventional MRI, suggesting that this technology could aid in localization and protection of nerves intraoperatively.

The oculomotor nerves (CN III) were better visualized at 7 T (M = 3.25), compared with 1.5 T (M = 2.28) and 3 T MRI (M = 2.5). Mass effect from an enlarging tumor may also compromise CN III, leading to oculomotor palsy in 2.4 to 17% of patients with anterior skull base tumors.[23] CN III might also be damaged intraoperatively, with oculomotor palsy in 2.8% of EES patients.[24] High-resolution preoperative imaging may facilitate preservation of oculomotor integrity in the 4% of cases where macroadenomas extend into the oculomotor cisterns.[23]

Ability to visualize the trochlear nerve (CN IV) was also greater at 7 T (M = 0.84) compared with conventional MRI (M = 0.09). Since this CN is the smallest by axon composition, it has historically been exceedingly difficult to identify radiologically. Damage to CN IV, resulting in trochlear paresis and diplopia, has been reported in 2.2% of adenoma resection patients.[25] Cheng et al used a high-resolution structural protocol that was optimized for imaging the skull base,

Table 3 Neuroradiological ratings of tumor depiction, cranial nerves, and internal carotid artery branches as well as Knosp's scores

	7 T ($n = 18$)	Clinical MRI ($n = 18$)	*p*-value	7 T ($n = 7$)	3 T ($n = 7$)	*p*-value	7 T ($n = 11$)	1.5 T ($n = 11$)	*p*-value
Depiction of tumor									
Tumor extension through bone	2.94	3.22	0.54	2.57	3.14	1.0	3.18	3.27	1.0
Optic chiasm compression	3.89	3.56	0.53	3.86	3.86	1.0	3.91	3.36	0.63
Cystic/necrotic/ hemorrhagic component	3.33	2.94	0.54	3.14	3.0	1.0	3.45	2.91	0.63
Tumor vasculature	1.88	1.61	0.54	1.83	1.57	1.0	1.91	1.64	0.85
R-medial cavernous sinus wall invasion	3.29	3.11	0.5	3.0	2.86	1.0	3.45	3.27	0.92
L-medial cavernous sinus wall invasion	3.35	3.0	0.54	3.17	2.71	1.0	3.45	3.18	0.85
Orbital involvement	3.41	3.56	0.54	2.83	3.43	1.0	3.73	3.63	1.0
Brain invasion	3.42	3.33	0.51	3.17	3.57	1.0	3.55	3.18	0.85
CNs									
CN II	3.23	3.28	1.0	3.0	3.29	0.81	3.45	3.27	0.75
CN III	3.25	2.37	**0.002**	3.08	2.5	**0.03**	3.36	2.28	**0.03**
CN IV	0.84	0.09	**0.002**	0.93	0.22	0.19	0.78	0.0	**0.04**
CN VI	0.95	0.52	**0.01**	0.93	0.71	0.83	0.96	0.38	**0.03**
ICA branches									
Ophthalmic	2.5	1.48	**0.03**	1.87	1.79	1.0	2.91	1.27	**0.01**
Superior hypophyseal	0.11	0.06	0.94	0.14	0.0	1.0	0.09	0.09	1.0
ACA	3.89	3.78	1.0	3.72	3.72	1.0	4.0	3.82	1.0
MCA	4.0	4.0	1.0	4.0	4.0	1.0	4.0	4.0	1.0
PCOM	2.72	2.2	**0.03**	3.93	1.93	0.75	2.59	2.37	0.35
Anterior choroidal	2.17	1.31	0.11	2.14	1.43	1.0	2.18	1.18	0.28
Supraclinoid ICA	4.0	4.0	1.0	4.0	4.0	1.0	4.0	4.0	1.0
R Knosp's score	1.06	1.17	1.0	0.57	0.57	1.0	1.36	1.55	1.0
L Knosp's score	1.44	0.89	0.54	1.29	0.57	0.75	1.55	1.09	1.0
Confidence in Knosp's rating	2.611	2.83	0.54	2.47	3.0	0.75	2.64	2.73	1.0

Abbreviations: ACA, anterior cerebral artery; CN, cranial nerve; ICA, internal carotid artery; L, left; MCA, middle cerebral artery; MRI, magnetic resonance imaging; PCOM, posterior communicating artery; R, right.
Note: bolded values indicate Bonferroni's adjusted *p*-values below 0.05. 0, structure was not seen; 1, poor visualization; 2, fair visualization; 3, good visualization; 4, excellent visualization.

and reported definite and probable visualization of CN IV in only 16 and 22% of healthy individuals, respectively.[26] In this study, CN IV was visualized (received a minimum rating of 1) in 10 patients (55.6%) at 7 T, whereas conventional MRI identified CN IV in only two of nine patients (11.1%), both at 3 T. While the ability to image CN IV was better at 7 T compared with conventional MRI, no significant effects were found compared with 1.5 or 3 T results separately. This disparity is attributable to a reduced subanalysis sample size, so future work may include validating these results with larger sample sizes.

The abducens nerve (CN VI) was better visualized at 7 T ($M = 0.95$) compared with conventional MRI ($M = 0.52$). CN VI palsy is the most commonly reported isolated cranial neuropathy. This nerve is particularly at risk during endoscopic surgery, since it is the most medially located within the cavernous sinus. Damage to CN VI during endoscopic surgery has been reported in 2 to 2.8,[24,27] resulting in ptosis, miosis, or other deficits. Because of the CN VI trajectory in the skull base, there have been many efforts to identify surgical landmarks to aid in localization intraoperatively.[28] Furthermore, tumor location relative to CN VI can inform surgical approach, since lesions posterolateral to the nerve may be best accessed through a lateral transcranial approach.[28] While cisternal CN VI can be seen with advanced conventional MRI sequences,[8] this nerve is rarely seen within the skull base using on conventional MRI. Increased visibility of CN VI at the skull base may be an important advantage of

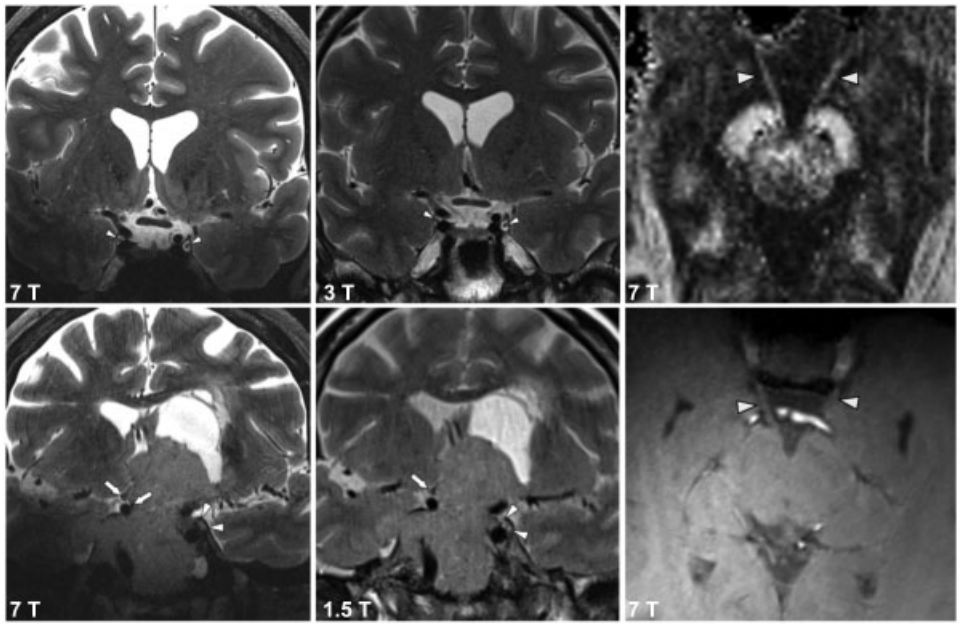

Fig. 1 Coronal T2-TSE depicting the oculomotor nerve (CN III). The left and middle columns show CN III at 7 T image compared with 3 and 1.5 T, respectively. The right column shows 7 T DTI FA image and a T1-weighted MP2RAGE inversion-2 sequence. The oculomotor nerves (denoted by white arrow heads) can be seen emerging from the interpedunclar fossa. Nerve visualization is better on the high spatial resolution (1.05 mm) isotropic diffusion imaging compared with the structural sequence. CN, cranial nerve; DTI, diffusion tensor imaging. FA, fractional anisotropy; MPRAGE, magnetization-prepared rapid acquisition with gradient echo.

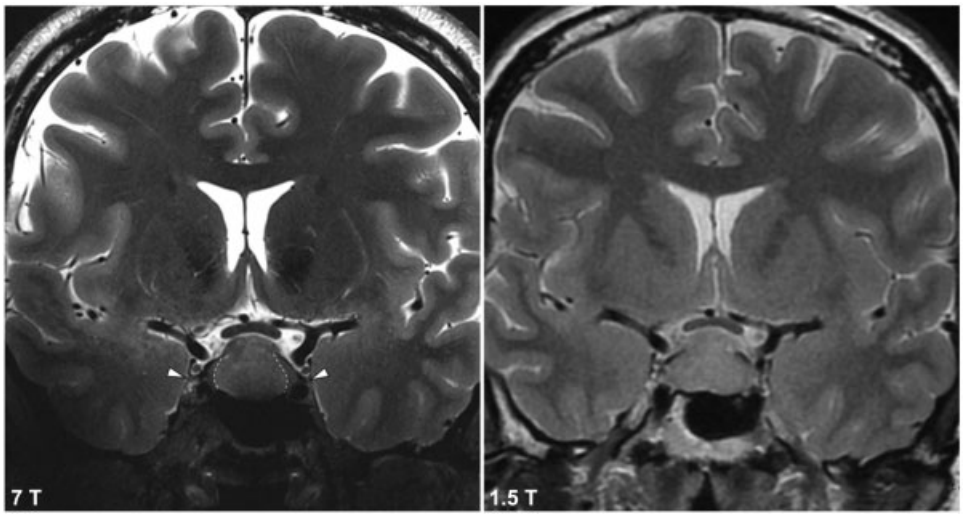

Fig. 2 Coronal T2-TSE depicting the trochlear nerve (CN IV) at 7 T (left) and 1.5 T (right). Dashed lines represents demarcation between central tumor or and preserved normal gland laterally. This boundary is not seen at 1.5 T. CN, cranial nerve.

7 T MRI for surgeons approaching the orbital fissure, clivus, and petroclival region either endoscopically or transcranially, as nerve characterization may reduce operative morbidity.

Together, these results suggest superiority of 7 T to conventional MRI in identification of certain CNs preoperatively, potentially aiding navigation and reducing postoperative cranial neuropathy in adenoma patients. Prospective randomized studies are warranted to evaluate postoperative outcomes and complications in patients undergoing 7, 3, and 1.5 T for surgical planning. Additionally, 3-T fast imaging employing steady-state acquisition (FIESTA) MRI has also shown to provide increased visualization of CNs and future work ought to compare CN detection between 7 T and lower field FIESTA imaging.[29] Technical development is still required to develop a 7 T FIESTA sequence; however, this is another promising area of advancement in the field of skull base imaging that may further benefit CN imaging. In the future, additional 7 T sequences may increase CN conspicuity. In particular, the high–isotropic spatial resolution (1.05 mm) afforded by ultra-high field diffusion MRI may facilitate superior depiction of smaller nerves at 7 T, thereby benefitting surgical planning as it has with the trigeminal nerve (CN V).[19] Visualization of CNs at 7 T should also be compared with steady-state free precession on conventional MRI that enhances at least cisternal nerve visualization.

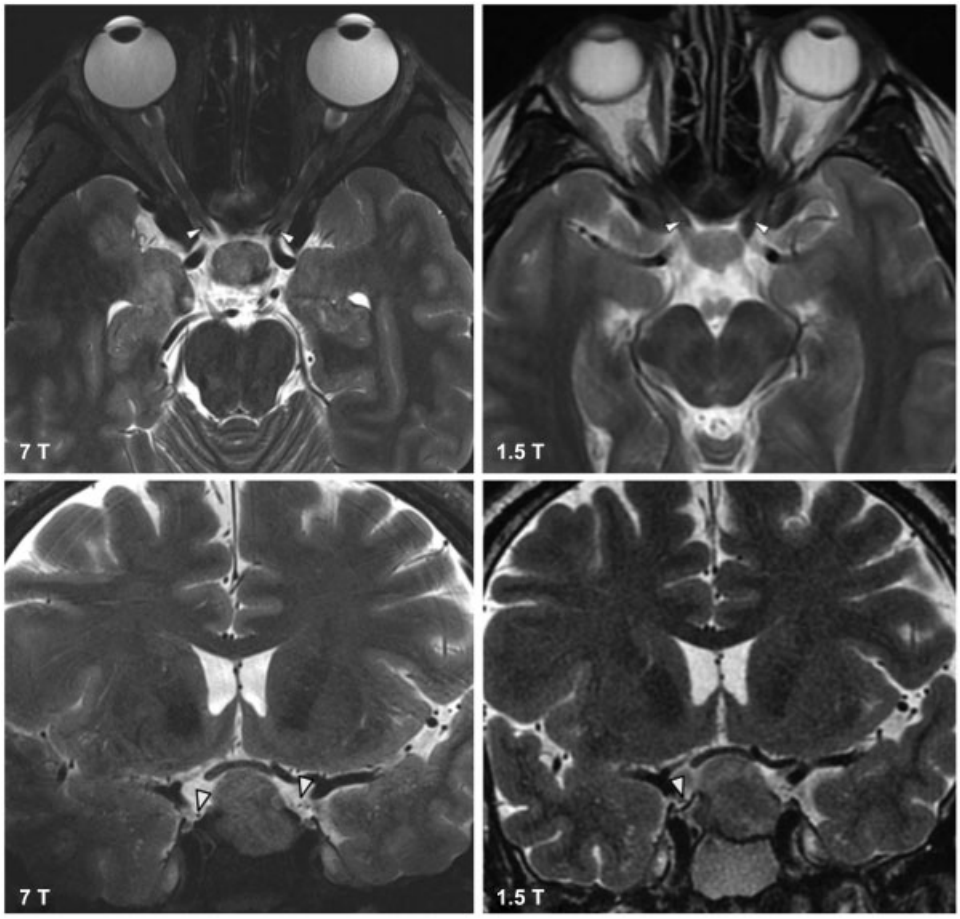

Fig. 3 The top row shows axial T2-TSE images of the ophthalmic artery at 7 T (left) and 1.5 T (right). The top row shows coronal T2-TSE images of the right posterior communicating artery (PCOM) at 7 T (left). The PCOM is not visible at 1.5 T (right).

Internal Carotid Artery Branches

Preoperative imaging of vascular anatomy is another important component of planning for adenoma EES. While ICA injury is rare (0.2–1.1% of hypophysectomy EES cases[30,31]), laceration to ICA branches can be rapidly catastrophic, profuse bleeding can quickly flood the surgical field thereby hampering subsequent hemostasis. Narrow access corridors and inability to suture further hinder limit the ability to control serious hemorrhage.[30] Even with adequate bleeding control, ICA branch injury can result in stroke, cranial neuropathy, and death.[30,32] Therefore, avoiding vascular injury is of paramount importance during EES, and improved preoperative definition of ICA branches could reduce ICA trauma and hemorrhage. Our high-spatial resolution 7 T TOF angiography (0.26 mm × 0.26 mm × 0.4 mm), which suppresses background signal by exploiting longer tissue T1 values, increases arterial contrast and small vessel detectability, and enables excellent visualization of skull base arteries without intravenous contrast.[10,33]

Ophthalmic arteries were better visualized at 7 T (M = 2.5) compared with conventional MRI (M = 1.48). This finding persisted against 1.5 T scans but not against 3 T scans. Ophthalmic artery damage comprises 7.3 to 25%[32,34] of all vascular injuries from endoscopic skull base surgery. In addition to challenges from surgical field obscuration, ophthalmic artery injury may lead to permanent vision loss.[35]

The posterior communicating arteries (PCOMs) were also better visualized at 7 T (M = 2.72) compared with conventional MRI (M = 2.2). Identification of PCOMs may be important for diverse skull base endoscopic procedures, such as the endoscopic approach to the foramen magnum and odontoid.[36] Future studies may demonstrate when vessel visualization may decrease morbidity with ultra-high field imaging.

Given the significant morbidity and mortality associated with ICA damage and the physical limitations associated with endoscopic repair of arterial injury, improved visualization of ICA branches might prove among the most important advantages conferred by 7 T over conventional MRI in this study. Enhanced visualization of the ophthalmic and PCOM arteries may be useful verifiable landmarks at 7 T that contribute to surgical safety, predict extent of resection, and avoid critical vasculature during resection of adenomas. Increased ICA branch visualization may benefit other endoscopic procedures, including extended endoscopic surgery of the clivus and petrous apex, where ICA injury is described in up to 9% of cases.[31] However, given the excellent visualization of arteries in this study, ultra-high field TOF acquisitions optimized for the skull base could obviate the need for contrast assessment of fine vessels. Quantitative yield of noncontrast 7 T MRI to contrast-enhanced imaging conventional MRI is an important line of inquiry and an area of active investigation.

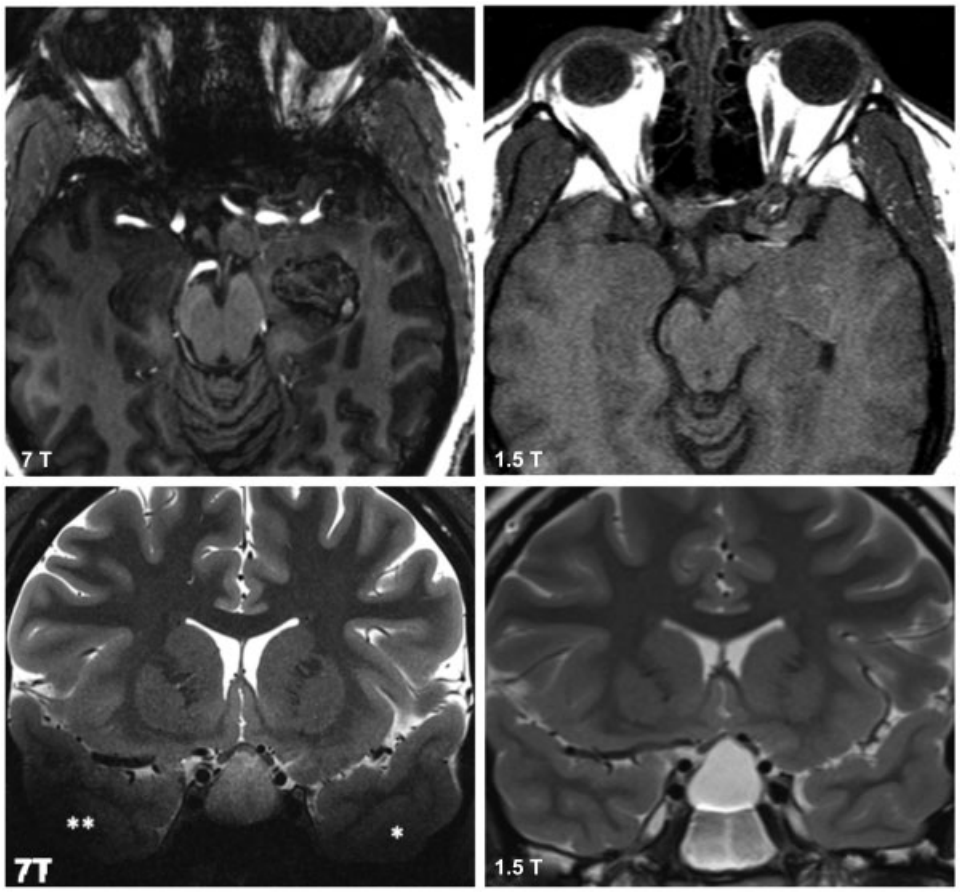

Fig. 4 Top row shows axial T1-weighted MPRAGE images with B0 inhomogeneity artifact more apparent at 7 T (left) than at 1.5 T (right) along the greater sphenoid wing and anterior skull base. Bottom row shows coronal T2-TSE images with B1 inhomogeneity artifact more apparent at 7 T (left) than at 1.5 T (right). Asterisks denote significant signal drop out in the temporal lobes due to B1 effects. DTI FA image and inversion MP2RAGE inversion 2. The oculomotor nerves can be seen emerging from the interpedunclar fossa better on diffusion compared with structural sequence. DTI, diffusion tensor imaging.

Artifacts and Overall Image Quality

Higher SNR is attainable at 7 T MRI compared with conventional MRI, since SNR scales with increasing magnetic field.[10] The higher SNR at 7 T can be leveraged to provide adequate resolution for fine structures typically challenging at conventional MRI, while maintaining reasonable scan times.[10]

While 7 T MRI offers increased SNR and spatial resolution, several physical limitations can compromise image quality. This study showed that B0 and B1 inhomogeneities are more apparent at 7 T compared with conventional MRI. B0 inhomogeneity, attributable to sensitivity-to-susceptibility effects with field strength, is particularly apparent at large air-tissue interfaces, such as along the margins of paranasal sinuses.[37] With a significant positive correlation between average overall diagnostic quality of each sequence and tumor volume, it appears that larger lesions may lessen B0 air-tissue interface artifact by diminishing artifact from air cavities. The utility of 7 T for imaging pituitary adenomas of different sizes is an important area of investigation and may indicate certain tumors properties that are optimally depicted by 7 T MRI. B1 inhomogeneity becomes increasingly troublesome at ultra-high field because the radiofrequency (RF) wavelength approaches the diameter of the head, leading to wave effects that cause variation in the transmitted field. Localized shimming methods and use of dielectric pads do mitigate the effects of B1 artifact at ultra-high field, and both were employed in this study. Despite these considerations, our study confirms that B1 inhomogeneity remains more severe at 7 T compared with conventional MRI. However, our results also showed superior visualization of many structures at ultra-high field, suggesting that increased SNR and spatial resolution at 7 T MRI may outweigh B0 and B1 inhomogeneity limitations. Evolution of hardware and engineering solutions, including high-order shimming methods for B0 artifacts and advanced adiabatic pulse design for B1 effects, may further expand the utility of 7 T MRI in skull base imaging.

Limitations and Future Directions

A notable limitation of the present study is the lack of standardization for conventional MRI. The clinical images compared against 7 T MRI were scans obtained at 1.5 (11/18) or 3 T (7/18) patients as part of standard-of-care evaluation. Although we compared 7 T MRI to the combined 1.5 and 3 T cohort as well, field strength-specific subanalyses were likely underpowered, and some significant effects may have been undetected. Future work will include recruiting more patients in the 1.5 and 3 T clinical imaging groups. Additionally, due to the conspicuity of 7 T MRI, lack of blinded

neuroradiological assessment is an inherent limitation in this study.

Another limitation was application of 7 T MRI for preoperative characterization of tumor and adjacent anatomy without intraoperative correlation. Intraoperative comparison of the utility of 7 T versus conventional MRI using current technology would pose technical challenges, hampered by inability to toggle across different data volumes in the operative suite, while maintaining stereotactic coregistration with endoscopic instruments. Collaboration with surgical navigation vendors will be important for adding 7 T display to coregistered navigation systems, thereby facilitating intraoperative comparison of field strength without interrupting surgical work flow, and this is an area of future investigation in our group. Similarly, the present study sought to examine benefits conferred by 7 T MRI in only the preoperative setting, and both 7 T and clinical field strength data were used for surgical decision making. Future prospective studies with patients that receive solely 7 or 3 T will be important for systematically compared long-term surgical outcomes and determine the role of ultrahigh field MRI in reducing operative morbidity and preserving endocrine function.

In addition to the technical and hardware development work required to overcome physical limitations of 7 T MRI, we believe that this work may advance other aspects of skull base neurosurgery. Since metabolic chemical shift magnitudes are proportional to magnetic field strength and excellent spectral separation and quantification is potentially attainable at 7 T,[10] ultra-high field MR spectroscopy may offer insights into adenoma composition. Indeed, quantitative MR spectroscopy has already provided important information about tumor proliferative index and perfusion properties in prior adenoma studies on conventional MRI.[38] Furthermore, high spectral-resolution metabolic signatures may help localize MRI-negative secreting microadenomas. 7 T MRI is well positioned to advance imaging paradigms for other neoplasms, including invasive features of malignant skull base tumors.[39] Since extensive tumor involvement with sensitive anterior skull base anatomy can preclude a purely endoscopic approach, the ability of 7 T MRI to characterize tumor infiltration of structures, such as the periorbita, ICAs, dura, and CNs should be examined in the context of surgical decision making for sinonasal malignancies. Ultra-high field imaging could also benefit the radiotherapeutic management of skull base malignancies, as high-resolution 7 T MRI may enhance lesion boundary visualization and permit dose modifications when appropriate. This application may be particularly valuable in the case of clival chordomas, where inadequate tumor delineation in proximity to the brainstem and cord can result in tumor underdosing.[40] The utility of 7 T MRI in the surgical and radiotherapeutic management of skull base malignancy is an important area of future investigation in this field.

Lastly, we report a relatively small number of structures that are better imaged at 7 T compared with clinical field strength MRI, and the question of whether the cost of this technology is justified by these advantages is an important consideration. With the recent 510 K approval of 7 T MRI from the FDA for clinical use, we anticipate an increase in the number of installation sites and a reduction in cost as these scanners are increasingly implemented into clinical work flow. Furthermore, because this preliminary study included a relatively small sample size, we cannot conclude with certainty that visualization of other skull base structures are not also benefitted by increased magnetic field strength, and additional studies are warranted to fully elucidate the role of 7 T in endoscopic pituitary surgery.

Conclusion

The present study is the first quantitative comparison of 7 T and conventional MRI for visualization of pituitary adenomas and adjacent neurovascular structures. These results demonstrate that 7 T MRI is feasible at the anterior skull base without inferiority to 1.5- or 3-T MRI. Visualization of many anterior skull base structures, including CNs and ICA branches was found with ultra-high field, suggesting that this modality may be useful for identifying landmarks and increasing surgical safety for skull base neurosurgery. It is expected that refinements of 7 T acquisition and signal readout methods will further reduce artifacts in this region, and that imaging quality in and about the skull base will continue to improve. Furthermore, it is believed that 7 T MRI demonstrates potential to have an increasingly important role in the optimal preoperative imaging and surgical management for patients with pituitary adenomas as well as other anterior skull base pathologies.

Funding
National Institutes of Health (grant/award number: NIH R01 CA202911).

Conflict of Interest
P.B. (the principal investigator in this study) is a named inventor on patents relating to MRI and RF pulse design. The patents have been licensed to GE Healthcare, Siemens AG, and Philips international. P.B. receives royalty payments relating to these patents.
P.B. is a named inventor on patents relating to slice-selective adiabatic magnetization T2-preparation (SAMPA) for efficient T2-weighted imaging at ultra-high field strengths, methods for producing a semiadiabatic spectral–spatial spectroscopic imaging sequence and devices Thereof, and semiadiabatic spectral–spatial spectroscopic imaging. These patents have been filed through MSIP; they remain unlicensed, there is no discussion to license them in the near future, and there are consequently no royalties revolving around them.
R.E.F. is a named inventor on patents relating to MRI and RF pulse design, semiadiabatic spectral–spatial spectro-spatial imaging (SASSI) and semiadiabatic matched phase spin echo power independent of the number of pulses (SEAMS PINS). She does not receive financial compensation related to these patents.
The remaining authors report no conflict of interest concerning the materials or methods used in this study or the findings specified in this paper.

References

1 Chatzellis E, Alexandraki KI, Androulakis II, Kaltsas G. Aggressive pituitary tumors. Neuroendocrinology 2015;101(02):87–104
2 Barzaghi LR, Losa M, Giovanelli M, Mortini P. Complications of transsphenoidal surgery in patients with pituitary adenoma: experience at a single centre. Acta Neurochir (Wien) 2007;149 (09):877–885, discussion 885–886
3 Cohen AR, Cooper PR, Kupersmith MJ, Flamm ES, Ransohoff J. Visual recovery after transsphenoidal removal of pituitary adenomas. Neurosurgery 1985;17(03):446–452
4 Jahangiri A, Wagner JR, Han SW, et al. Improved versus worsened endocrine function after transsphenoidal surgery for nonfunctional pituitary adenomas: rate, time course, and radiological analysis. J Neurosurg 2016;124(03):589–595
5 Agam M, Carmichael JD, Weiss MH, Zada G, Wedemeyer MA. 152 complications associated with transsphenoidal pituitary surgery: experience of 1171 consecutive cases treated at a single tertiary care pituitary center. Neurosurgery 2017;64(CN_suppl_1):237–237
6 Cappabianca P, Cavallo LM, Colao A, de Divitiis E. Surgical complications associated with the endoscopic endonasal transsphenoidal approach for pituitary adenomas. J Neurosurg 2002;97(02):293–298
7 Dolati P, Eichberg D, Golby A, Zamani A, Laws E. Multimodal navigation in endoscopic transsphenoidal resection of pituitary tumors using image-based vascular and cranial nerve segmentation: a prospective validation study. World Neurosurg 2016;95:406–413
8 Ono K, Arai H, Endo T, et al. Detailed MR imaging anatomy of the abducent nerve: evagination of CSF into Dorello canal. AJNR Am J Neuroradiol 2004;25(04):623–626
9 de Rotte AA, Groenewegen A, Rutgers DR, et al. High resolution pituitary gland MRI at 7.0 tesla: a clinical evaluation in Cushing's disease. Eur Radiol 2016;26(01):271–277
10 Balchandani P, Naidich TP. Ultra-high-field MR neuroimaging. AJNR Am J Neuroradiol 2015;36(07):1204–1215
11 Veersema TJ, Ferrier CH, van Eijsden P, et al. Seven tesla MRI improves detection of focal cortical dysplasia in patients with refractory focal epilepsy. Epilepsia Open 2017;2(02):162–171
12 Inglese M, Fleysher L, Oesingmann N, Petracca M. Clinical applications of ultra-high field magnetic resonance imaging in multiple sclerosis. Expert Rev Neurother 2018;18(03):221–230
13 Ali R, Goubran M, Choudhri O, Zeineh MM. Seven-Tesla MRI and neuroimaging biomarkers for Alzheimer's disease. Neurosurg Focus 2015;39(05):E4
14 Barrett TF, Dyvorne HA, Padormo F, et al. First application of 7-T magnetic resonance imaging in endoscopic endonasal surgery of skull base tumors. World Neurosurg 2017;103:600–610
15 Law M, Wang R, Liu C-SJ, et al. Value of pituitary gland MRI at 7 T in Cushing's disease and relationship to inferior petrosal sinus sampling: case report. J Neurosurg 2018;130(02):347
16 Tomayko MM, Reynolds CPJCC. Determination of subcutaneous tumor size in athymic (nude) mice. Cancer Chemother Pharmacol 1989;24(03):148–154
17 Haller S, Etienne L, Kövari E, Varoquaux AD, Urbach H, Becker M. Imaging of neurovascular compression syndromes: trigeminal neuralgia, hemifacial spasm, vestibular paroxysmia, and glossopharyngeal neuralgia. AJNR Am J Neuroradiol 2016;37(08):1384–1392
18 Jani RH, Hughes MA, Gold MS, Branstetter BF, Ligus ZE, Sekula RF Jr. Trigeminal nerve compression without trigeminal neuralgia: intraoperative vs imaging evidence. Neurosurgery 2019;84(01):60–65
19 Moon HC, You ST, Baek HM, et al. 7.0 Tesla MRI tractography in patients with trigeminal neuralgia. Magn Reson Imaging 2018; 54:265–270
20 Chen DQ, Quan J, Guha A, Tymianski M, Mikulis D, Hodaie M. Three-dimensional in vivo modeling of vestibular schwannomas and surrounding cranial nerves with diffusion imaging tractography. Neurosurgery 2011;68(04):1077–1083
21 Gerganov VM, Giordano M, Samii M, Samii A. Diffusion tensor imaging-based fiber tracking for prediction of the position of the facial nerve in relation to large vestibular schwannomas. J Neurosurg 2011;115(06):1087–1093
22 Jouanneau E, Jacquesson T, Bosc J, et al. Probabilistic tractography to predict the position of cranial nerves displaced by skull base tumors: value for surgical strategy through a case series of 62 patients. 2019;85(01):E125–E136
23 Hoang N, Tran DK, Herde R, Couldwell GC, Osborn AG, Couldwell WT. Pituitary macroadenomas with oculomotor cistern extension and tracking: implications for surgical management. J Neurosurg 2016;125(02):315–322
24 Woodworth GF, Patel KS, Shin B, et al. Surgical outcomes using a medial-to-lateral endonasal endoscopic approach to pituitary adenomas invading the cavernous sinus. J Neurosurg 2014;120 (05):1086–1094
25 Shkarubo AN, Chernov IV, Ogurtsova AA, et al. Cranial nerve monitoring in endoscopic endonasal surgery of skull base tumors (observing of 23 cases). Chinese Neurosurgical Journal. 2018;4(01):38
26 Cheng YS, Zhou ZR, Peng WJ, Tang F. Three-dimensional-fast imaging employing steady-state acquisition and T2-weighted fast spin-echo magnetic resonance sequences on visualization of cranial nerves III - XII. Chin Med J (Engl) 2008;121(03):276–279
27 Fernandez-Miranda JC, Zwagerman NT, Abhinav K, et al. Cavernous sinus compartments from the endoscopic endonasal approach: anatomical considerations and surgical relevance to adenoma surgery. J Neurosurg 2017;129(02):430–441
28 Barges-Coll J, Fernandez-Miranda JC, Prevedello DM, et al. Avoiding injury to the abducens nerve during expanded endonasal endoscopic surgery: anatomic and clinical case studies. Neurosurgery 2010;67(01):144–154, discussion 154
29 Mikami T, Minamida Y, Yamaki T, Koyanagi I, Nonaka T, Houkin K. Cranial nerve assessment in posterior fossa tumors with fast imaging employing steady-state acquisition (FIESTA). Neurosurg Rev 2005;28(04):261–266
30 Duek I, Sviri GE, Amit M, Gil Z. Endoscopic endonasal repair of internal carotid artery injury during endoscopic endonasal surgery. J Neurol Surg Rep 2017;78(04):e125–e128
31 Rowan NR, Turner MT, Valappil B, et al. Injury of the carotid artery during endoscopic endonasal surgery: surveys of skull base surgeons. J Neurol Surg B Skull Base 2018;79(03):302–308
32 Chin OY, Ghosh R, Fang CH, Baredes S, Liu JK, Eloy JA. Internal carotid artery injury in endoscopic endonasal surgery: A systematic review. Laryngoscope 2016;126(03):582–590
33 Bae KT, Park SH, Moon CH, Kim JH, Kaya D, Zhao T. Dual-echo arteriovenography imaging with 7T MRI. J Magn Reson Imaging 2010;31(01):255–261
34 Romero ADCB, Lal Gangadharan J, Bander ED, Gobin YP, Anand VK, Schwartz TH. Managing arterial injury in endoscopic skull base surgery: case series and review of the literature. Operative Neurosurgery 2016;13(01):138–149
35 Ambarki K, Hallberg P, Jóhannesson G, et al. Blood flow of ophthalmic artery in healthy individuals determined by phase-contrast magnetic resonance imaging. Invest Ophthalmol Vis Sci 2013;54(04):2738–2745
36 Kassam A, Snyderman CH, Mintz A, Gardner P, Carrau RL. Expanded endonasal approach: the rostrocaudal axis. Part II. Posterior clinoids to the foramen magnum. Neurosurg Focus 2005;19(01):E4
37 Vargas MI, Delavelle J, Kohler R, Becker CD, Lovblad K. Brain and spine MRI artifacts at 3Tesla. J Neuroradiol 2009;36(02):74–81
38 Stadlbauer A, Buchfelder M, Nimsky C, et al. Proton magnetic resonance spectroscopy in pituitary macroadenomas: preliminary results. J Neurosurg 2008;109(02):306–312
39 Mahalingappa YB, Khalil HS. Sinonasal malignancy: presentation and outcomes. J Laryngol Otol 2014;128(07):654–657
40 Förander P, Bartek J Jr, Fagerlund M, et al. Multidisciplinary management of clival chordomas; long-term clinical outcome in a single-institution consecutive series. Acta Neurochir (Wien) 2017;159(10):1857–1868

